

SIMS studies of planetary cumulates: Orthopyroxene from the Stillwater Complex, Montana

J. J. PAPIKE, M. N. SPILDE, G. W. FOWLER

Institute of Meteoritics, Department of Earth and Planetary Sciences, University of New Mexico, Albuquerque, New Mexico 87131-1126, U.S.A.

I. S. MCCALLUM

Department of Geological Sciences, University of Washington, Seattle, Washington 98195, U.S.A.

ABSTRACT

Igneous cumulate rocks provide an important record of planetary magmatism, but there are pitfalls in their interpretation. The rocks are composed of cumulus minerals plus assemblages that crystallized from trapped melt. Cumulus minerals may react with the trapped melt and other cumulus phases during subsolidus reactions, thus losing a direct record of their igneous history. One of the best approaches for estimating the melt compositions parental to the cumulates is to analyze the cores of cumulus phases for elements with slow diffusion rates (e.g., REE) because these most reliably retain a record of the mineral-melt partitioning.

Many of the cumulus orthopyroxene grains from the Stillwater Complex analyzed in this study have augite lamellae in their interiors but lamellae-free rims. Secondary ion mass spectrometer (SIMS) analysis shows that these orthopyroxene rims have lower Sr, Y, Zr, and Ce concentrations relative to the cores. These systematics were apparently caused by migration of augite exsolution lamellae, which preferentially incorporate these trace elements, out of the rims of the orthopyroxene grains.

SIMS analyses for REE in orthopyroxene cores show lower LREE concentrations, $(Ce/Yb)_n$, and $(Dy/Yb)_n$ than the isotope dilution data on mineral separates (Lambert and Simmons, 1987). We believe that these differences result from one or more contaminating phases (e.g., augite and plagioclase) in the orthopyroxene mineral separates. The SIMS data yield calculated parental melts similar to sills found below the Stillwater Complex, which have previously been suggested as possible parental melts (Helz, 1985).

A major focus of this study was to determine whether the onset of plagioclase crystallization at the bronzitite zone–norite zone contact was the result of fractionation until plagioclase saturation of the magmas parental to the bronzitites, or if mixing of a second magma with higher Al activity was the cause of plagioclase crystallization. The data presented in this paper, coupled with existing data, support the magma-mixing model.

INTRODUCTION

Igneous cumulate rocks provide an important record of planetary magmatism, but several factors must be considered when interpreting such rocks. The compositions of parental magmas may have been modified by polybaric fractional crystallization, contamination, and magma mixing. The compositions of cumulus minerals may have been modified by reaction with trapped intercumulus liquid during cooling. Furthermore, primary mineral compositions may be locally changed in response to subsolidus reequilibrium. Separation and quantification of these effects requires detailed information on mineral zoning profiles.

We have conducted electron microprobe (EMP) and secondary ion mass spectrometer (SIMS) studies of pyroxenes from a variety of planetary cumulates, including lunar norites (Papike et al., 1994) and asteroidal ortho-

pyroxenites (diogenites, Fowler et al., 1994, 1995). As an extension of this work, we present in this paper data on orthopyroxene from sample suites from the Mountain View and Lost Mountain localities (Figs. 1–4) of the Stillwater Complex, Montana.

Orthopyroxene is a very useful mineral recorder in mafic cumulates, as demonstrated by Lambert and Simmons (1987), who used REE data from orthopyroxene crystals to calculate the melt compositions that crystallized to form the various cumulate layers in the Stillwater Complex. Two aspects of this research particularly intrigued us. Lambert and Simmons (1987) used a sequential grinding procedure to isolate the cores of cumulus orthopyroxene grains to remove trace element-rich rims produced by crystallization of intercumulus liquid after the system became closed. The finer abraded material (–200 mesh) showed significantly higher REE relative to the coarser (100–200 mesh) fraction, which was assumed to repre-

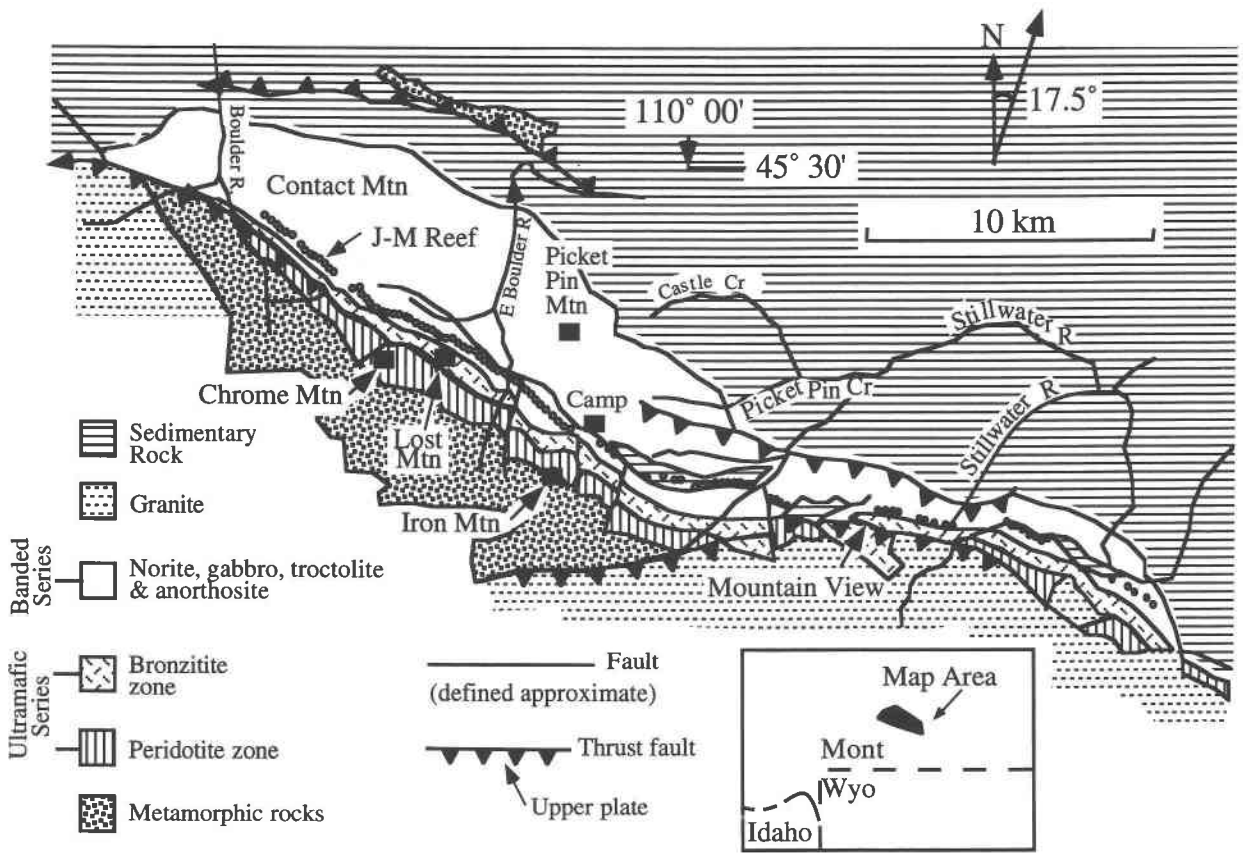


Fig. 1. Generalized geologic map of the Stillwater Complex, Montana (after Lambert and Simmons, 1987).

sent the cores of the pyroxene grains. Preliminary studies of core-to-rim variations in Stillwater pyroxenes reported by Spilde et al. (1993b) failed to reveal these enriched rims. The second result of the Lambert and Simmons (1987) study that we wished to explore was the elevated light REE they observed for their orthopyroxene separates. We felt that further insights could be obtained on the trace element characteristics of Stillwater orthopyroxenes by studying them with a microbeam instrument such as SIMS.

A comprehensive review of previous work on the Stillwater Complex is provided in Czamanske and Zientek (1985). The Stillwater Complex, located in southwestern Montana, strikes NW-SE approximately parallel with the north margin of the Beartooth Mountains and dips steeply to the north (Fig. 1). The age of the complex is 2701 ± 8 Ma (DePaolo and Wasserburg, 1979). The complex is divided into a basal series, an ultramafic series, and a banded series (Fig. 2). The boundary between the basal series and the ultramafic series is marked by the appearance of cumulus olivine, whereas the lowest boundary of the banded series is defined as the horizon where plagioclase first appears as a cumulus phase. The ultramafic series is subdivided into a lower peridotite zone in which olivine or olivine + orthopyroxene are the cumulus min-

erals and an upper bronzitite zone in which orthopyroxene is the only cumulus mineral. Orthopyroxene in the entire bronzitite zone is remarkably constant in composition (Fig. 3), with $Mg/(Mg + Fe)$ atomic = 85 ± 1 (Raedeke and McCallum, 1984). Raedeke and McCallum concluded that simple fractional crystallization, plus crystal settling, is not sufficient to explain the lithologic sequences observed in the ultramafic series. They proposed a model in which accretion of cumulates and growth of the magma chamber proceeded through periodic influxes of olivine-saturated basaltic magma that initially pooled on or near the chamber floor. Fe-enrichment trends that would result from fractionation were suppressed by the effects of repeated injections of new magma, extrusion of fractionated magma, periodic equilibrium crystallization, and reaction of cumulates with trapped liquid.

Lambert and Simmons (1987) presented isotope dilution analyses of REE and microprobe analyses of 17 cumulus orthopyroxene separates from the ultramafic series. They concluded that the ultramafic series formed by multiple injection and fractional crystallization of magmas derived from the upper mantle by a dynamic melting process. These magmas were characterized by having rather high $(Ce/Yb)_n$ ratios of 8–18. Subscript *n* refers to the normalization of elemental abundances to chondritic

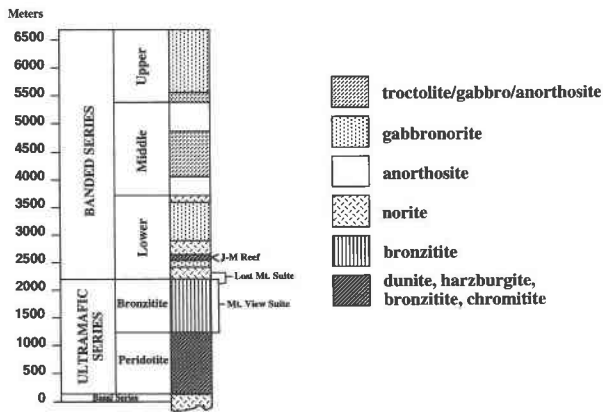


Fig. 2. Generalized stratigraphic section of the Stillwater Complex, Montana, based on the stratigraphic sections of McCallum et al. (1980) and Raedeke and McCallum (1984).

values (Anders and Grevesse, 1989). Lambert and Simmons concluded that either the mantle source region was light REE enriched or the partial melts were contaminated by light REE-enriched crustal rocks.

The bronzite zone–norite zone contact is of particular interest because it is the most prominent contact in the complex. It can be traced across the entire strike length and is marked by the abrupt appearance of cumulus plagioclase. However, this contact is not as simple as it appears at first glance, and it has been interpreted as (1) the result of normal fractionation as the magma reached plagioclase saturation (Hess, 1960), (2) the horizon at which suspended plagioclase began to accumulate on the floor of the chamber (McCallum et al., 1980), or (3) the product of an influx of a batch of plagioclase-saturated magma (Lambert, 1982; Thurber and McCallum, 1990). Raedeke (1982) compared the compositions of orthopyroxene on both sides of the contact and observed a decrease in Mg/(Mg + Fe) (~4 mol%), Cr₂O₃, and Al₂O₃ from the bronzite to the norite zone. In the immediate vicinity of the contact, however, the compositional differences are less pronounced. Lambert and Simmons (1987, 1988) observed a distinct discontinuity in relative abundances of REE in plagioclase across the contact, which is particularly striking in LREE abundance, e.g., (Ce/Sm)_n = 5.2–5.5 and (Nd/Sm)_n = 2.2–2.3 in intercumulus plagioclase from bronzite in comparison with (Ce/Sm)_n = 3.1–3.5 and (Nd/Sm)_n = 1.8–1.9 in cumulus plagioclase from norite. However, we must remember that we are comparing cumulus vs. intercumulus plagioclase. LREE variations are much less pronounced in orthopyroxene.

Pegmatitic patches, discordant anorthositic segregations, and isoclinally folded layering are common in the lowermost norite, and several samples collected from the actual contact contain a thin (1–3 mm) layer of chromite between the norite and bronzite. Thurber and McCallum (1990) proposed that the chromite layer may be the result of the influx of a hotter plagioclase-saturated magma that thermally eroded bronzite cumulates, re-

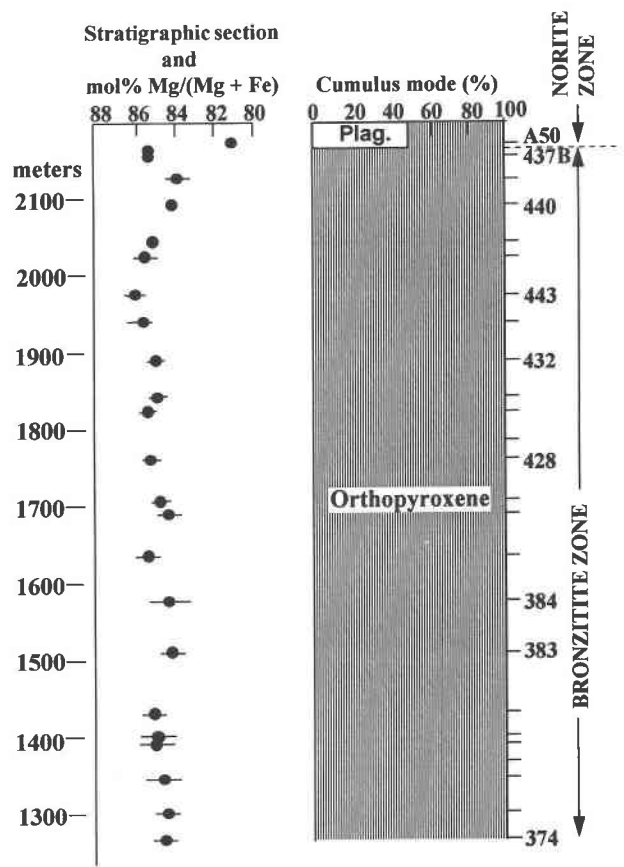


Fig. 3. The Mountain View sample suite, Stillwater Complex, Montana. Locations of samples analyzed and Mg/(Mg + Fe) values from Raedeke and McCallum (1984). The bronzite zone starts at 1260 m above the base of the complex. Note Fig. 2.

leasing Cr, which then precipitated as chromite at the reaction front.

EXPERIMENTAL METHODS

Major and minor elements in orthopyroxene were analyzed using a JEOL 733 Superprobe equipped with five wavelength-dispersive spectrometers (WDS) and an Oxford/Link energy-dispersive system (EDS), controlled by an Oxford eXL II operating system. All analyses were performed using an accelerating voltage of 15 kV and a beam current of 20 nA. A beam diameter of 5 μm or greater was used to reintegrate fine (100) augite lamellae during analysis of pyroxene interiors. Core and rim analyses were conducted using EDS for major elements (Mg, Si, and Fe) and WDS for minor and trace elements (Na, Al, Ca, Ti, Cr, and Mn). High-quality minerals were used as standards for both WDS calibration and for reference EDS profiles. Test analyses were performed on secondary mineral standards to determine the quality of calibration and analysis error. EDS spectra were collected for 75 s to acquire over 150 000 counts in the full spectrum, thus providing good counting statistics. WDS peak counting times of 20–30 s for minor and trace elements were ac-

cumulated simultaneously with the EDS spectrum. ZAF corrections were applied to all microprobe analyses. Core-only analyses prior to SIMS investigation were conducted under the same conditions except that all nine elements were analyzed by WDS with major element counting times of 20 s and minor and trace element counting times of 30 s. Experiments conducted in our laboratory indicate that using a combined EDS-WDS analytical package saves analysis time and still provides highly reproducible analyses with low error (e.g., relative major element < 3%).

For our SIMS studies we selected nine samples from the Mountain View locality, including eight from the bronzitite zone of the ultramafic series and one from the base of the norite zone, and a sequence of seven samples from the Lost Mountain locality, which represent the bronzitite-norite zone contact between the ultramafic series and the lower banded series (Figs. 1–4).

SIMS analyses of orthopyroxene were conducted using a Cameca IMS 4f ion microprobe. Orthopyroxene from the Mountain View transect (Fig. 3) was analyzed for the minor elements Ca, Na, Al, Ti, Cr, and Mn, and the trace elements V, Sr, Y, Zr, Ce, and Yb (first analytical package). Orthopyroxene grains from both the Mountain View transect and the Lost Mountain transect were analyzed for a more complete set of trace elements Sr, Y, Zr, La, Ce, Nd, Sm, Eu, Dy, Er, and Yb (second analytical package). For clarity in plotting REE patterns with Eu anomalies, concentrations of Gd were estimated using simple interpolation between Sm and Dy.

Analyses were made by bombardment of the sample with primary O^- ions accelerated through a nominal potential of 10 kV. A primary ion current of 30–40 nA was focused on the sample over a spot diameter of 25–35 μm . Sputtered secondary ions were energy filtered using an energy window of ± 25 V and sample offset voltages of -105 and -75 V, respectively, for the first and second analytical packages described above. This degree of energy filtering effectively eliminates the effect of isobaric interferences for the elements analyzed in this study (Shimizu et al., 1978).

Each analysis involved repeated cycles of peak counting on $^{40}\text{Ca}^{2+}$, $^{23}\text{Na}^+$, $^{27}\text{Al}^+$, $^{30}\text{Si}^+$, $^{47}\text{Ti}^+$, $^{51}\text{V}^+$, $^{52}\text{Cr}^+$, $^{55}\text{Mn}^+$, $^{88}\text{Sr}^+$, $^{89}\text{Y}^+$, $^{90}\text{Zr}^+$, $^{93}\text{Nb}^+$, $^{140}\text{Ce}^+$, and $^{174}\text{Yb}^+$ (first package) or $^{30}\text{Si}^+$, $^{88}\text{Sr}^+$, $^{89}\text{Y}^+$, $^{90}\text{Zr}^+$, $^{139}\text{La}^+$, $^{140}\text{Ce}^+$, $^{146}\text{Nd}^+$, $^{147}\text{Sm}^+$, $^{151}\text{Eu}^+$, $^{153}\text{Eu}^+$, $^{163}\text{Dy}^+$, $^{167}\text{Er}^+$, and $^{174}\text{Yb}^+$ (second package). Use of the $^{40}\text{Ca}^{2+}$ peak ($m/q \approx 20$) allows for analysis of Ca in orthopyroxene by avoiding the substantial isobaric interference from $^{24}\text{Mg}^{16}\text{O}^+$ present on the $^{40}\text{Ca}^+$ peak. Both packages included counting on a background position to monitor detector noise. Absolute concentrations of each element were then calculated using empirical relationships between measured $\text{peak}/^{30}\text{Si}^+$ ratios (normalized to known SiO_2 content) and elemental concentrations, as derived from daily calibration measurements of the documented pyroxene standards Kilbourne Hole augite (Irving and Frey, 1984) and Kakanui augite (Mason and Allen, 1973).

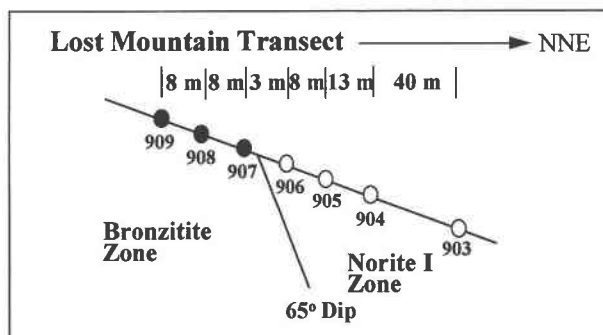


Fig. 4. The Lost Mountain sample suite, Stillwater Complex, Montana.

Peak counting times were varied to optimize precision. For the REEs, precisions are typically better than 5–10% at concentrations of $1 \times$ chondrite. In the case of the other trace and minor elements, precision is typically better than 1–2%.

All ion microprobe analyses were conducted at locations previously analyzed by EMP, and the SiO_2 concentrations determined by EMP were used in reducing the SIMS data. Inclusion of contaminating phases in the SIMS analyses was avoided by selecting optically clean orthopyroxene grains and by mass imaging of major elements before and after each SIMS spot analysis. Clean core areas were selected and, with the exception of the core and rim pairs of analyses for the Mountain View transect, rims of orthopyroxene grains were avoided. Approximately five SIMS analyses were obtained per thin section, each from the core of an individual orthopyroxene grain.

RESULTS

Orthopyroxene core-to-rim systematics

For this portion of our study, four samples were selected from a suite of eight samples spanning 900 m of the bronzitite zone of the ultramafic series. The samples represent the bottom (sample 374), the middle (428, 432), and the top (437B) of the zone from the Mountain View locality (Fig. 3). The reader is referred to Raedeke and McCallum (1984) for a complete petrographic description of the bronzitite and related zones. The analyzed samples consist of subhedral to euhedral orthopyroxene (bronzite) and minor amounts ($\sim 10\%$) of interstitial plagioclase and augite. The large, cumulus orthopyroxene grains nearly always contain augite exsolution lamellae. Commonly, fine lamellae, submicrometer to a few micrometers in width, occur on the (100) planes of the orthopyroxene. In addition to fine exsolution lamellae within the orthopyroxene grains, larger, blebby clinopyroxene inclusions are present; the large inclusions may be tens of micrometers in breadth and length. These inclusions appear to thicken at the expense of (100) augite lamellae because there are regions surrounding the inclusions that contain no lamellae. These blebby augites are interpreted

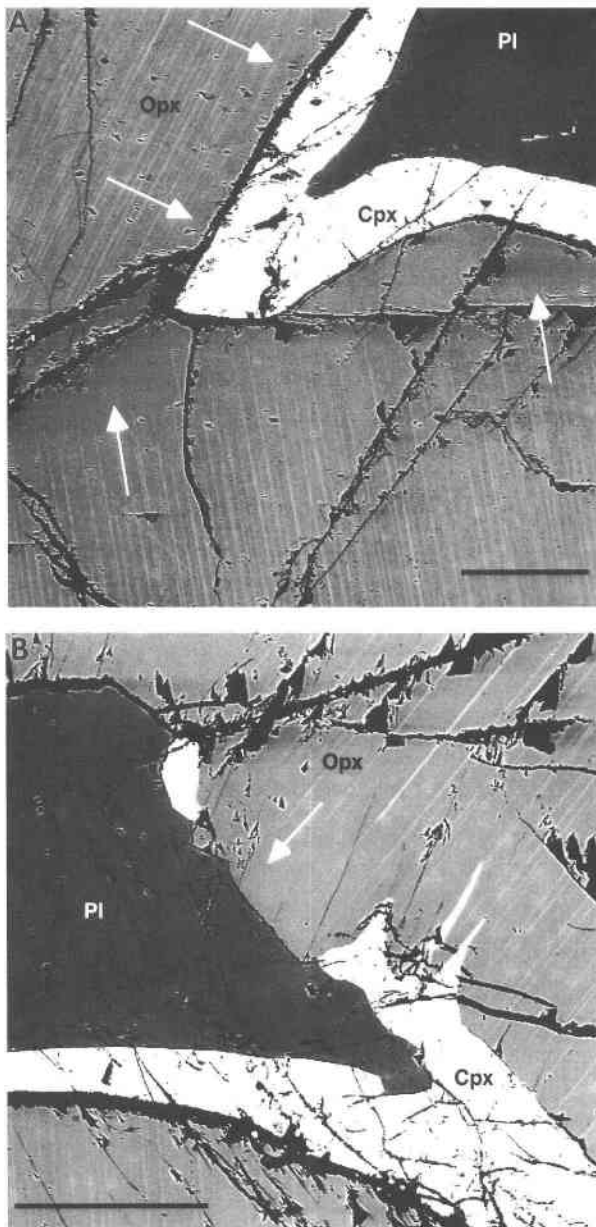


Fig. 5. Backscattered electron (BSE) images showing examples of lamellae-free zones at the rims of orthopyroxene (Opx), shown in medium gray. Clinopyroxene (Cpx) is white and plagioclase (Pl) is dark gray. Scale bars are 100 μm . (A) Fine lamellae on the (100) planes of orthopyroxene are visible in both crystals but stop short of the crystal rims, indicated by the arrows. (B) Coarse and fine lamellae are visible in the orthopyroxene crystal in the upper right but are absent at the rim (arrow). Note the fingers of coarse clinopyroxene that extend into the orthopyroxene, representing lamellae that have coalesced and bled into the rimming augite.

to have formed from the original, thinner, (100) augite lamellae.

Irregular, interstitial augite crystals typically occur along orthopyroxene grain boundaries and at the juncture of

TABLE 1. Average microprobe analyses of Cpx hosted in orthopyroxene in sample 428

| | Rim <i>n</i> = 8 | Bleb <i>n</i> = 8 | Lamella <i>n</i> = 2 |
|--------------------------------|---------------------|----------------------|-------------------------|
| SiO ₂ (wt%) | 53.8(4) | 53.1(4) | 53.9(2) |
| Al ₂ O ₃ | 1.4(1) | 1.8(2) | 1.3(7) |
| TiO ₂ | 0.18(3) | 0.15(3) | 0.12(1) |
| Cr ₂ O ₃ | 0.90(8) | 1.03(8) | 0.82(4) |
| MgO | 16.7(9) | 16.3(2) | 16.9(1) |
| FeO | 3.0(2) | 3.2(1) | 3.0(2) |
| MnO | 0.07(2) | 0.09(2) | 0.09(2) |
| CaO | 23.8(2) | 23.3(2) | 23.4(1) |
| Na ₂ O | 0.27(2) | 0.33(2) | 0.31(1) |
| Total oxide | 100.18 | 99.37 | 99.93 |
| Si (afu) | 1.960 | 1.950 | 1.967 |
| ^{IV} Al | 0.040 | 0.050 | 0.033 |
| Total tetrahedral | 2.000 | 2.000 | 2.000 |
| ^{VI} Al (afu) | 0.022 | 0.028 | 0.022 |
| Ti | 0.005 | 0.004 | 0.003 |
| Cr | 0.026 | 0.030 | 0.024 |
| Mg | 0.905 | 0.895 | 0.919 |
| Fe | 0.091 | 0.098 | 0.092 |
| Mn | 0.002 | 0.003 | 0.003 |
| Ca | 0.930 | 0.920 | 0.916 |
| Na | 0.019 | 0.024 | 0.022 |
| Total M1 + M2 | 2.001 | 2.003 | 2.001 |
| Mg/(Mg + Fe) | 0.908 | 0.901 | 0.909 |
| Wo | 48.3 | 48.1 | 47.5 |
| En | 47.0 | 46.8 | 47.7 |
| Fs | 4.75 | 5.14 | 4.79 |

Note: Parentheses indicate standard deviation in last decimal place.

several grains. This type of augite is distinct from larger intercumulus crystals that occur in some samples in that this rimming augite is narrower and does not contain orthopyroxene lamellae (Fig. 5A and 5B). Representative microprobe analyses of a wide lamella, blebby inclusions, and rimming augite are given in Table 1.

The fine lamellae typically occur throughout the bronzite grains. However, there are many regions at the rims of the bronzite crystals where no lamellae are present (Fig. 5A and 5B). SIMS analyses indicate that certain trace element concentrations are significantly lower within these zones. The abundance of selected trace elements in the cores and rims of crystals from four samples are given in Table 2. In all cases, the rims that exhibit a lack of lamellae show a decrease in selected trace elements relative to the core analyses (Fig. 6). This trend is evident across the bronzite zone in each of the grains analyzed from all four samples.

The observation of lower REE at orthopyroxene rims apparently contradicts the results of Lambert and Simmons (1987), who used an abrasion technique to remove the outer portion of the orthopyroxene crystals. They observed a significant increase in all REE in their abraded (rim) fraction and attributed the increase of REE at the orthopyroxene rims to the closed-system crystallization of a trapped intercumulus liquid (Lambert and Simmons, 1987).

SIMS analysis of an augite bleb in an orthopyroxene grain and a rimming augite next to another grain indicates that the augite displays elevated REE relative to the orthopyroxene (Table 2 and Fig. 7). The excess REE ob-

TABLE 2. Average trace element analyses by SIMS(2)* of cores and rims of orthopyroxene and selected augite blebs in four samples from the Mountain View transect

| Sample | 437B | | 432 | | 428 | | 374 | | 432 | 428 |
|----------|-------|-------|-------|-------|-------|-------|-------|-------|---------|----------|
| | Core | Rim | Core | Rim | Core | Rim | Core | Rim | Cpx Rim | Cpx Bleb |
| Sr (ppm) | 0.299 | 0.169 | 0.207 | 0.135 | 0.260 | 0.168 | 0.417 | 0.111 | 5.67 | 23.4 |
| Y | 1.37 | 1.10 | 1.58 | 1.04 | 2.13 | 1.45 | 1.57 | 1.00 | 10.8 | 20.8 |
| Zr | 1.77 | 1.42 | 2.24 | 1.34 | 2.15 | 1.47 | 1.20 | 0.59 | 20.4 | 36.9 |
| La | — | — | — | — | — | — | — | — | 0.554 | 1.9 |
| Ce | 0.078 | 0.024 | 0.084 | 0.018 | 0.162 | 0.046 | 0.043 | 0.011 | 2.48 | 7.1 |
| Nd | — | — | — | — | — | — | — | — | 2.45 | 5.7 |
| Sm | — | — | — | — | — | — | — | — | 0.856 | 2.2 |
| Eu | — | — | — | — | — | — | — | — | 0.317 | 0.6 |
| Dy | 0.136 | 0.128 | 0.160 | 0.101 | 0.215 | 0.137 | 0.183 | 0.096 | 1.60 | 3.4 |
| Er | 0.134 | 0.124 | 0.139 | 0.087 | 0.215 | 0.126 | 0.216 | 0.093 | 0.835 | 1.8 |
| Yb | 0.173 | 0.198 | 0.187 | 0.187 | 0.261 | 0.193 | 0.304 | 0.221 | 0.791 | 1.5 |

Note: Missing data not determined.

* SIMS(2) refers to the second SIMS analytical package; see Experimental Methods section of text.

served by Lambert and Simmons (1987) is possibly due to the inclusion of augite grains in their finer fraction.

Many bronzite grains and surrounding minerals display evidence of alteration along cracks and grain bound-

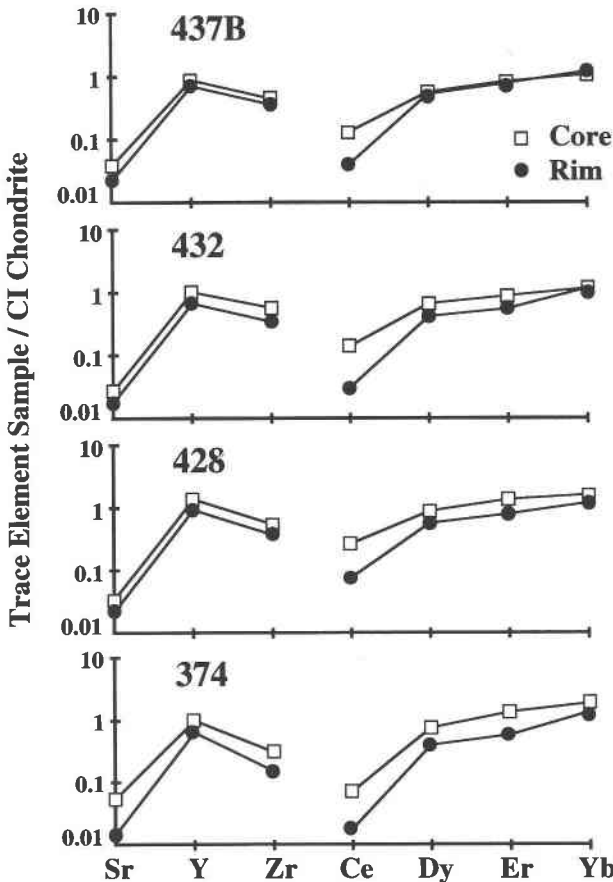


Fig. 6. Core vs. rim orthopyroxene analysis for four samples from the Mountain View sample suite. The rims, which are free of optically visible augite exsolution lamellae, have significantly lower Ce and slightly lower Sr, Y, Zr, Dy, Er, and Yb than the cores. Note the Experimental Methods section of the paper for an estimate of analytical errors. Normalized to chondrite data of Anders and Grevesse (1989).

aries. Figure 8 shows epidote occurring at the boundary between plagioclase and orthopyroxene. Furthermore, the pyroxene exhibits fractures that appear to have widened by dissolution of the orthopyroxene, whereas the augite lamellae appear relatively undisturbed. This selective alteration is typical of Stillwater rocks and is very similar to incipient pyroxene breakdown observed by Spilde et al. (1993a) in volcanic fumaroles at Katmai, Alaska. At that locality, low-pH, Cl-rich fluids reacted preferentially with orthopyroxene along cleavages and fractures, but clinopyroxene was not readily attacked. In addition to epidote precipitation, some grain boundaries show evidence of Fe concentrations, probably in the form of iron oxides. No discrete mineral phases were observed; the presence of Fe was indicated by element imaging on both the SIMS and the microprobe. The Lost Mountain suite appears to be more extensively altered than the Mountain View suite, with alteration extending to the interior of the crystals.

Bronzite and norite zones

More than 850 high-quality microprobe analyses of orthopyroxene were collected from a nine-sample Mountain View suite and a seven-sample Lost Mountain suite. All the acceptable analyses had to pass the following tests: (1) The oxide total must be between 98 and 102 wt%; (2) Si + Al must obey the relationship $1.98 < (Si + {}^{[4]}Al) < 2.02$ atoms per formula unit (afu); (3) the sum of the

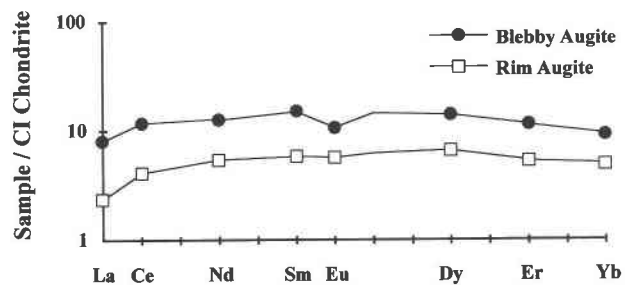


Fig. 7. Two chondrite-normalized REE patterns for augite from sample 428. See text for discussion and Tables 1 and 2 for major, minor, and trace element data.

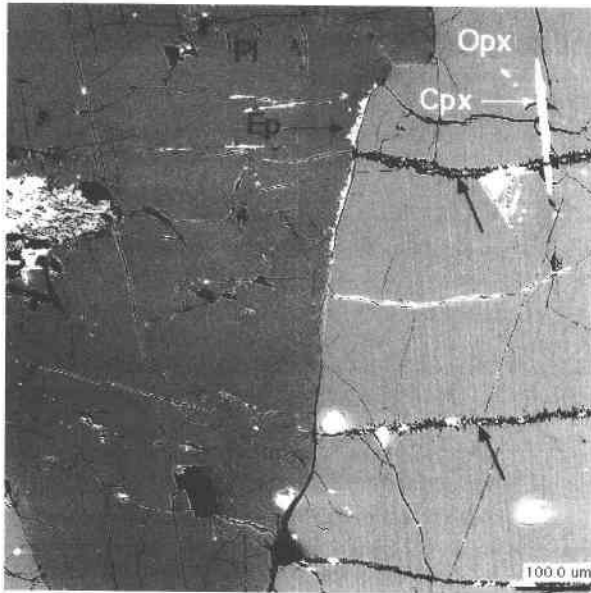


Fig. 8. In this BSE image, a large blebby inclusion of clinopyroxene is present within the orthopyroxene, parallel to the fine lamellae. A lamellae-free zone occurs step-wise along the rim of the orthopyroxene crystal. Epidote (Ep) occurs within plagioclase and at the grain boundary with orthopyroxene. Note the presence of horizontal fractures (at arrows) that appear to have been widened by preferential dissolution of the orthopyroxene, whereas the clinopyroxene exsolution lamellae are relatively unaffected, extending into the fracture like teeth. The bright circular features are SIMS pits containing residual gold coating from previous SIMS analyses.

cations (normalized to six O atoms) occupying the M2 and M1 sites must be between 1.98 and 2.02 (afu); and $(4) \text{Cr} + 2\text{Ti} \leq \text{Al}$ (afu) (Fowler et al., 1994). Average orthopyroxene major and minor analyses (~50 EMP analyses per sample) and trace analyses are tabulated in Tables 3–6. Figure 9 is a series of histograms that illustrate some major and minor element differences between orthopyroxene grains from the norite and bronzitite zones. For the Mountain View traverse (Fig. 3), eight samples are from the bronzitite zone, and only one is from the norite zone. Therefore, the bar heights for the bronzitite zone samples were reduced by a factor of eight to be more comparable to the one sample (A50) from the norite zone. For the Lost Mountain traverse (Fig. 4), the sampling is more evenly distributed, with four from the norite zone and three from the bronzitite zone. It is clear that there are some significant differences in the compositions of orthopyroxene from the norite zone and the bronzitite zone, with orthopyroxene in the norite zone having higher Ti and lower Cr, Al, and $\text{Mg}/(\text{Mg} + \text{Fe})$ atomic ratio. At least two models must be considered when explaining these systematics: (1) fractionation of a single magma that led to plagioclase saturation or (2) mixing of a second magma.

Figure 10 presents average (~5 SIMS analyses per grain), chondrite-normalized, orthopyroxene REE plots for the Lost Mountain traverse. Table 6 lists the SIMS data. Although there are some differences between REE patterns from the norite zone and bronzitite zone, there is not a simple regular sequence from the stratigraphically lowest sample, 909, to the stratigraphically highest sample, 903. Sample 903 appears anomalous because of its low REE content and lower LREE/HREE ratio. This lack of simple systematics was also observed by Lambert and Simmons (1987). Nevertheless, the orthopyroxene REE patterns from the norite zone generally show deeper negative Eu anomalies. In comparing our SIMS results with the Lambert and Simmons (1987) isotope dilution data, it is apparent that their REE patterns for orthopyroxene show considerably higher LREE than we observe (Fig. 11). Figure 12 shows more clearly the differences between the SIMS data and isotope dilution data in a $(\text{Ce}/\text{Yb})_n$ vs. $(\text{Dy}/\text{Yb})_n$ diagram (Lambert et al., 1994). The isotope dilution data plot at significantly higher $(\text{Ce}/\text{Yb})_n$ and $(\text{Dy}/\text{Yb})_n$ than the SIMS data. In Figure 12A we plot an augite analysis to see what effect contaminating augite in an orthopyroxene mineral separate might have. The isotope dilution data plot on a mixing line between our SIMS orthopyroxene and augite points. Mass balance and mixing calculations indicate that approximately 5 wt% of augite added to the SIMS orthopyroxene REE analyses produces parallel patterns for the SIMS and isotope dilution data. However, augite contamination also increases the total abundance of all the REE. Nevertheless, we do not want to push these calculations too far because we do not know if augite is the only contaminating phase; it is likely that some feldspar was also included in the orthopyroxene separates.

Also plotted on Figure 12B is the calculated orthopyroxene for two sills found beneath the Stillwater Complex that may represent parental melts of these Stillwater cumulates (Helz, 1985; Lambert and Simmons, 1988). One of them (sample NB 18/378) plots within the SIMS data cluster, and the other (VC81-23) plots near the cluster. Figure 13 provides a further comparison of the SIMS and isotope dilution data on a $(\text{Ce}/\text{Yb})_n$ histogram. The most direct comparison is for the Lost Mountain suite of samples, which were analyzed by both techniques. Again, the isotope dilution data indicate significantly higher $(\text{Ce}/\text{Yb})_n$ for orthopyroxene than the SIMS data.

Figure 14 illustrates estimated melt REE compositions on the basis of both the SIMS and isotope dilution data and REE data for the two candidate parental-melt sills (Helz, 1985). The data for the sills are from Lambert and Simmons (1988). The partition coefficients, from Lambert and Simmons (1987), used for these calculations are as follows: $\text{Ce} = 0.006$, $\text{Nd} = 0.011$, $\text{Sm} = 0.024$, $\text{Gd} = 0.046$, $\text{Dy} = 0.087$, $\text{Er} = 0.141$, and $\text{Yb} = 0.229$. The differences between the isotope dilution and SIMS data for orthopyroxene are reflected in the slopes of the calculated REE patterns. The Lambert and Simmons (1987)

TABLE 3. Average major and minor element analyses by EMP of Mountain View orthopyroxene

| Sample | A50 | 437B | 440 | 443 | 432 | 428 | 384 | 383 | 374 |
|--------------------------------|-------|-------|--------|--------|-------|-------|--------|-------|-------|
| SiO ₂ (wt%) | 55.4 | 55.4 | 55.8 | 56.0 | 55.2 | 56.0 | 56.3 | 55.1 | 55.3 |
| Al ₂ O ₃ | 1.21 | 1.82 | 1.49 | 1.48 | 1.44 | 1.39 | 1.32 | 1.43 | 1.74 |
| TiO ₂ | 0.16 | 0.10 | 0.09 | 0.11 | 0.09 | 0.11 | 0.10 | 0.12 | 0.08 |
| Cr ₂ O ₃ | 0.39 | 0.61 | 0.55 | 0.59 | 0.56 | 0.57 | 0.54 | 0.57 | 0.57 |
| MgO | 28.7 | 29.7 | 30.1 | 31.0 | 30.4 | 30.5 | 30.6 | 30.1 | 29.8 |
| FeO | 12.0 | 9.2 | 9.8 | 8.7 | 9.5 | 9.0 | 10.0 | 10.1 | 9.9 |
| MnO | 0.25 | 0.16 | 0.24 | 0.15 | 0.26 | 0.16 | 0.22 | 0.22 | 0.21 |
| CaO | 1.78 | 2.36 | 1.94 | 1.98 | 1.64 | 1.82 | 1.49 | 1.77 | 1.63 |
| Na ₂ O | 0.02 | 0.04 | 0.02 | 0.02 | 0.02 | 0.02 | 0.02 | 0.02 | 0.04 |
| Total oxide | 99.85 | 99.28 | 100.03 | 100.06 | 99.14 | 99.56 | 100.63 | 99.38 | 99.27 |
| Si (afu) | 1.972 | 1.962 | 1.965 | 1.961 | 1.960 | 1.971 | 1.970 | 1.957 | 1.961 |
| ⁴¹ Al | 0.028 | 0.038 | 0.035 | 0.039 | 0.040 | 0.029 | 0.030 | 0.043 | 0.039 |
| Total tetrahedral | 2.000 | 2.000 | 2.000 | 2.000 | 2.000 | 2.000 | 2.000 | 2.000 | 2.000 |
| ⁶³ Al (afu) | 0.022 | 0.038 | 0.027 | 0.022 | 0.020 | 0.029 | 0.025 | 0.017 | 0.034 |
| Ti | 0.004 | 0.003 | 0.002 | 0.003 | 0.002 | 0.003 | 0.003 | 0.003 | 0.002 |
| Cr | 0.011 | 0.017 | 0.015 | 0.016 | 0.016 | 0.016 | 0.015 | 0.016 | 0.016 |
| Mg | 1.521 | 1.564 | 1.579 | 1.620 | 1.609 | 1.602 | 1.594 | 1.592 | 1.577 |
| Fe | 0.359 | 0.271 | 0.290 | 0.256 | 0.282 | 0.264 | 0.293 | 0.299 | 0.294 |
| Mn | 0.007 | 0.005 | 0.007 | 0.004 | 0.008 | 0.005 | 0.007 | 0.007 | 0.006 |
| Ca | 0.068 | 0.091 | 0.073 | 0.075 | 0.062 | 0.069 | 0.056 | 0.067 | 0.062 |
| Na | 0.001 | 0.003 | 0.002 | 0.002 | 0.001 | 0.001 | 0.001 | 0.001 | 0.003 |
| Total M1 + M2 | 1.994 | 1.991 | 1.995 | 1.998 | 2.001 | 1.990 | 1.993 | 2.002 | 1.994 |
| Mg/(Mg + Fe) | 0.809 | 0.852 | 0.845 | 0.864 | 0.851 | 0.858 | 0.845 | 0.842 | 0.843 |
| Wo | 3.49 | 4.73 | 3.78 | 3.82 | 3.19 | 3.57 | 2.87 | 3.44 | 3.21 |
| En | 78.1 | 81.2 | 81.3 | 83.1 | 82.4 | 82.8 | 82.0 | 81.3 | 81.6 |
| Fs | 18.4 | 14.1 | 14.9 | 13.1 | 14.4 | 13.6 | 15.1 | 15.2 | 15.2 |

estimated melts (norite samples LM01 and LM02 and bronzitite samples LM04 and LM05) have higher LREE than those calculated from the SIMS data (norite samples 904 and 905 and bronzitite samples 907 and 908). The calculated melt for bronzitite samples 907 and 908 is quite similar to that of Mg-rich gabbronorite sill NB 18/378. It is apparent that melts calculated from orthopyroxene isotope dilution data have higher LREE than those calculated from the SIMS data.

The downward inflection of Ce in the combined pattern for samples 904 and 905 (Fig. 14) may be the result of the prior crystallization of plagioclase from melts parental to the norite. This is also seen in Figure 15 where the norite samples 903–906 have lower (Ce/Yb)_n than the bronzitite samples 907–909.

Figure 15 summarizes some of the trace element systematics for the two sample suites. In examining this diagram we should take into account that the nine-sample

suite from Mountain View spans ~900 m of stratigraphic section, whereas the seven-sample suite, from Lost Mountain, spans only 80 m across the bronzitite-norite zone contact. The (Ce/Yb)_n values are presented as a slope index for the REE patterns. Although the variations with stratigraphic height are not systematic, average (Ce/Yb)_n is lower in the norite zone than in the bronzitite zone. In the Mountain View traverse it is evident that sample A50 (norite) has significantly higher Zr, Y, and Yb than do the samples from the bronzitite zone. There is also some evidence of this in the Lost Mountain traverse but with much more scatter.

DISCUSSION

Orthopyroxene core-to-rim systematics

Sr, Y, Zr, and REE concentrations are lower at the orthopyroxene rims, which correlates to areas of the crys-

TABLE 4. Average minor and trace element analyses by SIMS(1)* of Mountain View transect orthopyroxene

| Sample | A50 | 437B | 440 | 443 | 432 | 428 | 384 | 383 | 374 |
|--------------------------------|-------|-------|-------|-------|-------|-------|-------|-------|-------|
| CaO (wt%) | 1.54 | 1.68 | 1.61 | 1.61 | 1.60 | 1.25 | 1.79 | 1.82 | 1.62 |
| Na ₂ O | 0.012 | 0.020 | 0.013 | 0.015 | 0.012 | 0.009 | 0.020 | 0.020 | 0.016 |
| Al ₂ O ₃ | 0.94 | 1.63 | 1.39 | 1.34 | 1.29 | 1.34 | 1.27 | 1.34 | 1.69 |
| TiO ₂ | 0.127 | 0.071 | 0.073 | 0.099 | 0.085 | 0.096 | 0.093 | 0.090 | 0.075 |
| V ₂ O ₅ | 0.023 | 0.018 | 0.021 | 0.020 | 0.019 | 0.019 | 0.021 | 0.020 | 0.018 |
| Cr ₂ O ₃ | 0.349 | 0.592 | 0.587 | 0.607 | 0.569 | 0.571 | 0.564 | 0.602 | 0.596 |
| MnO | 0.221 | 0.205 | 0.220 | 0.198 | 0.210 | 0.207 | 0.215 | 0.207 | 0.213 |
| Sr (ppm) | 0.213 | 0.265 | 0.254 | 0.227 | 0.154 | 0.169 | 0.395 | 0.402 | 0.268 |
| Y | 3.22 | 1.20 | 1.35 | 1.61 | 1.17 | 1.48 | 2.52 | 2.31 | 1.11 |
| Zr | 4.37 | 1.53 | 0.86 | 1.62 | 1.35 | 1.60 | 2.61 | 2.75 | 0.87 |
| Ce | 0.088 | 0.058 | 0.053 | 0.081 | 0.035 | 0.056 | 0.138 | 0.171 | 0.051 |
| Yb | 0.470 | 0.183 | 0.216 | 0.232 | 0.206 | 0.221 | 0.356 | 0.305 | 0.228 |

* SIMS(1) refers to the first SIMS analytical package; see Experimental Methods section of text.

TABLE 5. Average major and minor element analyses by EMP of Lost Mountain orthopyroxene

| Sample | 903 | 904 | 905 | 906 | 907 | 908 | 909 |
|--------------------------------|-------|-------|-------|-------|-------|-------|-------|
| SiO ₂ (wt%) | 55.3 | 55.0 | 54.9 | 55.1 | 55.2 | 55.2 | 55.1 |
| Al ₂ O ₃ | 1.21 | 1.15 | 1.15 | 1.43 | 1.33 | 1.22 | 1.49 |
| TiO ₂ | 0.19 | 0.21 | 0.22 | 0.13 | 0.18 | 0.21 | 0.11 |
| Cr ₂ O ₃ | 0.33 | 0.38 | 0.39 | 0.49 | 0.55 | 0.54 | 0.54 |
| MgO | 29.2 | 28.5 | 28.6 | 28.6 | 29.0 | 29.7 | 30.2 |
| FeO | 11.6 | 12.1 | 12.1 | 11.3 | 11.2 | 11.3 | 10.1 |
| MnO | 0.26 | 0.25 | 0.25 | 0.22 | 0.24 | 0.24 | 0.22 |
| CaO | 1.14 | 1.33 | 1.55 | 1.95 | 1.65 | 1.48 | 1.76 |
| Na ₂ O | 0.00 | 0.01 | 0.02 | 0.02 | 0.02 | 0.02 | 0.01 |
| Total oxide | 99.21 | 98.97 | 99.20 | 99.26 | 99.43 | 99.97 | 99.56 |
| Si (afu) | 1.974 | 1.976 | 1.969 | 1.970 | 1.968 | 1.958 | 1.954 |
| ²⁷ Al | 0.026 | 0.024 | 0.031 | 0.030 | 0.032 | 0.042 | 0.046 |
| Total tetrahedral | 2.000 | 2.000 | 2.000 | 2.000 | 2.000 | 2.000 | 2.000 |
| ²⁷ Al (afu) | 0.025 | 0.024 | 0.018 | 0.030 | 0.024 | 0.010 | 0.017 |
| Ti | 0.005 | 0.006 | 0.006 | 0.004 | 0.005 | 0.006 | 0.003 |
| Cr | 0.009 | 0.011 | 0.011 | 0.014 | 0.015 | 0.015 | 0.015 |
| Mg | 1.554 | 1.525 | 1.528 | 1.522 | 1.542 | 1.572 | 1.596 |
| Fe | 0.346 | 0.364 | 0.365 | 0.337 | 0.335 | 0.336 | 0.299 |
| Mn | 0.008 | 0.008 | 0.008 | 0.007 | 0.007 | 0.007 | 0.007 |
| Ca | 0.044 | 0.051 | 0.060 | 0.075 | 0.063 | 0.056 | 0.067 |
| Na | 0.000 | 0.001 | 0.001 | 0.001 | 0.001 | 0.001 | 0.001 |
| Total M1 + M2 | 1.990 | 1.989 | 1.996 | 1.990 | 1.992 | 2.004 | 2.005 |
| Mg/(Mg + Fe) | 0.818 | 0.807 | 0.807 | 0.819 | 0.822 | 0.824 | 0.842 |
| Wo | 2.25 | 2.64 | 3.06 | 3.91 | 3.25 | 2.87 | 3.41 |
| En | 80.0 | 78.6 | 78.3 | 78.7 | 79.5 | 80.0 | 81.4 |
| Fs | 17.8 | 18.8 | 18.7 | 17.4 | 17.3 | 17.1 | 15.2 |

tals that have no exsolution lamellae. It is well known that REEs are preferentially distributed into Ca-rich pyroxene relative to Ca-poor pyroxene (cf. McKay, 1989). Furthermore, SIMS work by Pun and Papike (1995) indicates that as augite exsolves from a pigeonite structure, the REEs become enriched in the Ca-rich lamellae and are decreased in the Ca-poor remnant. This phenomenon appears to affect the LREE to a greater extent than the HREE. Therefore, the presence of augite influences bulk REE analysis and should be taken into account when analyzing only orthopyroxene. Apart from a rim of a few tens of micrometers in width, the orthopyroxene shows a uniform distribution of (100) augite lamellae. Rims are easily avoided in SIMS analyses.

Lambert and Simmons (1987) concluded that the REE increased at the rims of the cumulus pyroxene. However, their analytical technique involved physically grinding the

mineral separates and analyzing the coarser fraction by bulk isotope dilution on the assumption that the fine fraction contained rim material. By utilizing the high spatial resolution of the SIMS ion beam (25–35 μm), we were able to analyze the orthopyroxene rims *in situ*, and our results are significantly different from those of the bulk technique. The increase in LREE that Lambert and Simmons observed could be the result of augite being incorporated into their analyses instead of the result of trapped melt crystallization. Augite is intimately attached to the exterior of orthopyroxene crystals. It is inevitable that some of this augite does not become completely separated from the bronzite grains.

As the presence of Ca-rich pyroxene increases REE in the analysis, the lack of Ca-rich lamellae at the orthopyroxene rim causes localized decreases in REE. The lower REE observed at the rims with a SIMS technique results from the partitioning of the REE into Ca-rich exsolution lamellae (Fig. 5A and 5B). The lamellae swept up much of the REE during exsolution, so those areas at the crystal rims without lamellae exhibit lower REE concentrations. Subsolidus coalescence of exsolution lamellae into larger lamellae is a common phenomenon. Indeed, lamellae have been observed to distort into large blebs, such as those observed by Bonnicksen (1969) in metamorphic pyroxenes in the Biwabik Iron Formation. Moreover, Pun and Papike (1995) observed very wide lamellae (tens of micrometers) and wormy intergrowths of Ca-rich pyroxene, which they attributed to distortion of lamellae. Migration of pyroxene lamellae out of a host crystal could occur during the slow cooling and annealing that would have taken place in the thick Stillwater cumulate pile. Therefore, we postulate that the lack of lamellae and the de-

TABLE 6. Average trace element analyses by SIMS(2)* of Lost Mountain orthopyroxene

| Sample | 903 | 904 | 905 | 906 | 907 | 908 | 909 |
|----------|-------|-------|-------|-------|-------|-------|-------|
| Sr (ppm) | 0.142 | 0.205 | 0.170 | 0.204 | 0.174 | 0.161 | 0.166 |
| Y | 2.35 | 3.92 | 4.58 | 2.61 | 3.28 | 3.72 | 1.49 |
| Zr | 4.28 | 4.58 | 5.80 | 4.42 | 4.19 | 3.38 | 1.94 |
| La | 0.006 | 0.021 | 0.018 | 0.016 | 0.039 | 0.044 | 0.020 |
| Ce | 0.035 | 0.120 | 0.118 | 0.095 | 0.156 | 0.212 | 0.066 |
| Nd | 0.051 | 0.185 | 0.227 | 0.123 | 0.201 | 0.256 | 0.097 |
| Sm | 0.037 | 0.123 | 0.146 | 0.068 | 0.088 | 0.146 | 0.071 |
| Eu | 0.009 | 0.015 | 0.023 | 0.014 | 0.022 | 0.039 | 0.015 |
| Dy | 0.222 | 0.474 | 0.661 | 0.290 | 0.374 | 0.373 | 0.155 |
| Er | 0.227 | 0.415 | 0.499 | 0.306 | 0.305 | 0.372 | 0.163 |
| Yb | 0.346 | 0.530 | 0.600 | 0.365 | 0.430 | 0.442 | 0.210 |

* SIMS(2) refers to the second SIMS analytical package; see Experimental Methods section in text.

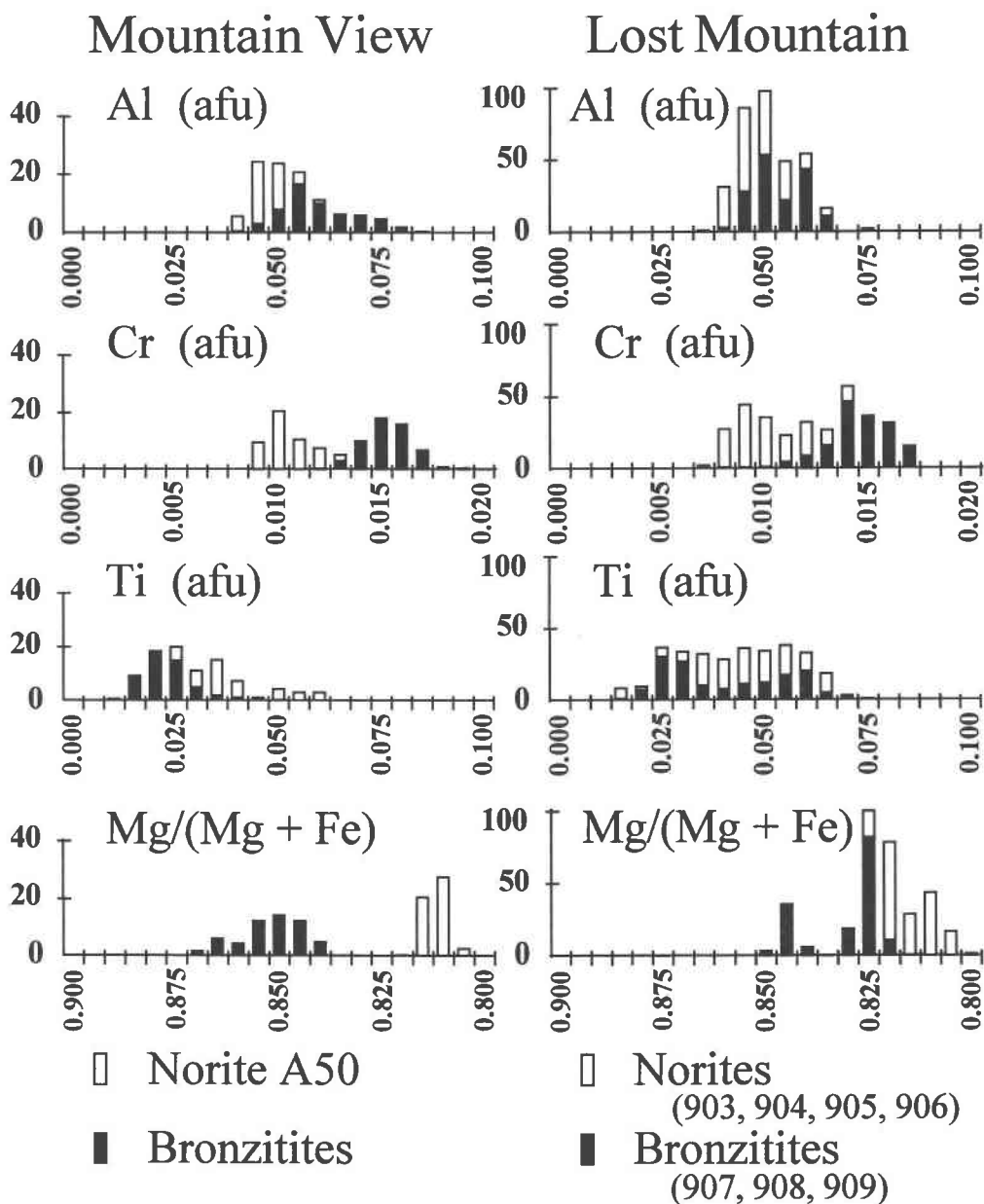


Fig. 9. Histograms of EMP data for Mountain View and Lost Mountain sample suites. Open bars represent norites and solid bars represent bronzites. Data presented in Tables 3 and 5. Afu = atoms per formula unit.

crease of REE at the orthopyroxene rims are due to this effect. The totally exsolved augite lamellae appear to have coalesced into the rimming augite that occurs along bronzite grain boundaries and at triple junctions (Fig. 5A and 5B).

Differences between isotope dilution data and SIMS data for orthopyroxene

The results presented above demonstrate that the isotope dilution technique yields higher LREE than the SIMS method for Stillwater orthopyroxene. We feel that this difference may be the result of contamination of the orthopyroxene mineral separates. Small amounts of plagioclase and augite in the orthopyroxene separates lead to higher LREE. The extent to which HREEs are affected depends on the relative amounts of plagioclase and augite in the contaminant. Any significant decrease in HREE requires plagioclase to be the dominant contaminant. Loferski and Arculus (1993) studied multiphase mineral inclusions in plagioclase from the Stillwater Complex and pointed out the problems the inclusions could cause when mineral separates are analyzed. A careful examination of Lost Mountain orthopyroxene failed to locate any significant inclusions. However, all orthopyroxene grains show some evidence of secondary alteration to tremolite ± talc

clase and augite in the orthopyroxene separates lead to higher LREE. The extent to which HREEs are affected depends on the relative amounts of plagioclase and augite in the contaminant. Any significant decrease in HREE requires plagioclase to be the dominant contaminant. Loferski and Arculus (1993) studied multiphase mineral inclusions in plagioclase from the Stillwater Complex and pointed out the problems the inclusions could cause when mineral separates are analyzed. A careful examination of Lost Mountain orthopyroxene failed to locate any significant inclusions. However, all orthopyroxene grains show some evidence of secondary alteration to tremolite ± talc

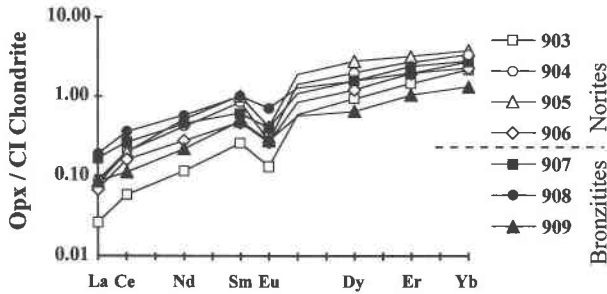


Fig. 10. Chondrite-normalized REE for orthopyroxene from the Lost Mountain sample suite. Data presented in Table 6. REEs are normalized to the chondrite data of Anders and Grevesse (1989).

± serpentine, which are impossible to separate mechanically. The extent to which this alteration assemblage would affect LREE is not well constrained. Finally, Stosch (1982) found that fluid inclusions in mantle orthopyroxene can contain high concentrations of incompatible trace elements, including LREE. He concluded that this may be responsible for unexpectedly high concentrations of incompatible trace elements for mantle olivine or orthopyroxene. However, fluid inclusions are very rare in Stillwater minerals and have never been observed in pyroxenes. Kurat et al. (1980) also found significant incompatible trace element enrichments in ultramafic xenoliths and attributed these enrichments to contamination from “percolating liquids.”

In a study of fine-grained mafic rocks from sills and dikes associated with the Stillwater Complex, Helz (1985) states with reference to the Lambert (1982) REE patterns: “As yet, no rocks have been found that show REE patterns so steep, or so depleted in heavy REE’s as those Lambert (1982) inferred for most of the Ultramafic-series liquids.” If the Lambert (1982) REE patterns were af-

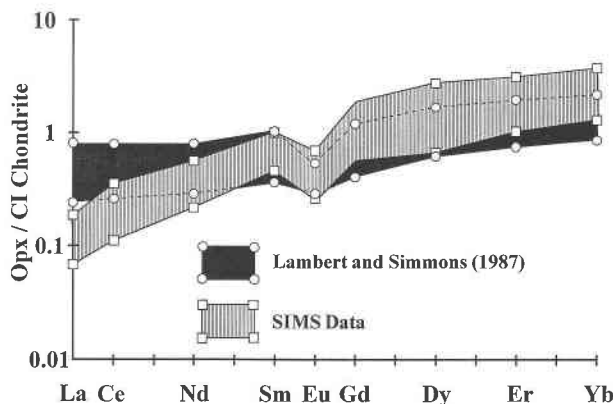
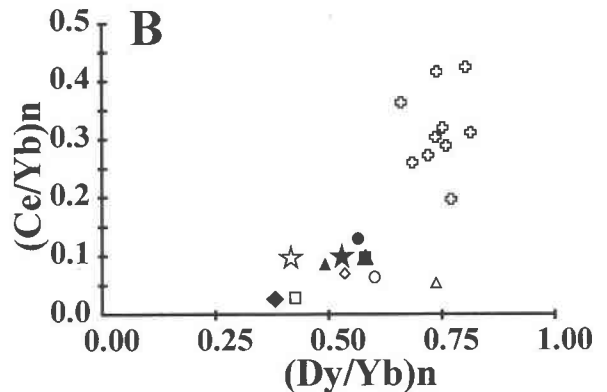
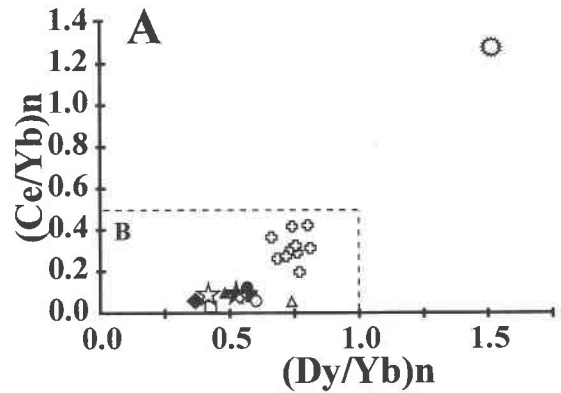


Fig. 11. Comparison of ranges of chondrite-normalized REE determined by isotope dilution (Lambert and Simmons, 1987) and SIMS (this study) for Lost Mountain orthopyroxenes. The pattern for sample 903 is omitted from the range because it is anomalous.



- 903 ■ 907 ⊕ Lambert and Simmons (1987)
- 904 ● 908 Lost Mtn. Data
- △ 905 ▲ 909 ★ NB 18/378 Opx
- ◇ 906 ◆ Chondritic Opx ☆ VC81-23 Opx
- (with dot) Blebby Augite

Fig. 12. Orthopyroxene $(Ce/Yb)_n$ vs. $(Dy/Yb)_n$ systematics. Isotope dilution data (Lambert and Simmons, 1987) and SIMS data (this study) are compared. Estimated $(Ce/Yb)_n$ and $(Dy/Yb)_n$ for orthopyroxene that would crystallize from Stillwater sills NB 18/378 and VC81-23 are also plotted. Orthopyroxene crystallizing from a chondritic melt (Anders and Grevesse, 1989) is shown for reference. Partition coefficients are reported in the text. (A) Augite plots in the upper right corner. The result of intercumulus augite contamination of cumulus orthopyroxene mineral separates would cause analytical results to plot on a mixing line between the group of orthopyroxenes from this study and the augite. B is a magnified view of the lower left portion of A.

ected by contamination (e.g., intercumulus augite and plagioclase), then the REE patterns of the main body of melt would have been somewhat flatter than the patterns they proposed. In summary, there is a difference between the isotope dilution and SIMS results for REE in Stillwater orthopyroxenes. The isotope dilution technique has greater accuracy and precision than the SIMS technique, but the approach can be compromised by contaminated mineral separates.

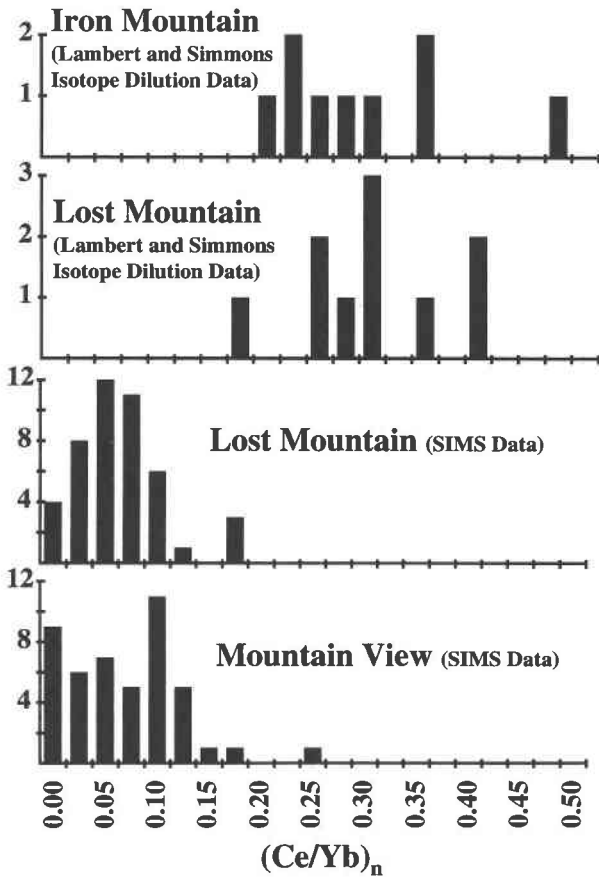


Fig. 13. $(Ce/Yb)_n$ histograms for orthopyroxene from isotope dilution data (Lambert and Simmons, 1987) and SIMS data (this study). See text for discussion. SIMS data presented in Tables 4 and 6.

Ultramafic series-banded series contact

As discussed in the introduction, one objective of this study was to provide a test of the various hypotheses that have been proposed to explain the sharp contact between the bronzitites of the ultramafic series and norites of the banded series. Before evaluating the data, however, it is important to quantify the effect of postcumulus reequilibration on the composition of cumulus minerals because the magnitude of the postcumulus shift on orthopyroxene would be significantly different in bronzitite containing ~90% orthopyroxene relative to norite containing ~40% orthopyroxene. In a protocumulate in which 90% bronzite reacts with 10% gabbro-noritic intercumulus melt, there would be a decrease in $Mg/(Mg + Fe)$ in orthopyroxene of ~0.8 mol%, whereas in a protonorite in which 35% bronzite + 55% plagioclase reacts with an intercumulus liquid of the same composition and amount, the decrease in $Mg/(Mg + Fe)$ would be ~2 mol% (calculation methods are outlined in Raedeke and McCallum, 1980). Ten percent melt is an upper limit for the amount of intercumulus liquid at the time of closure.

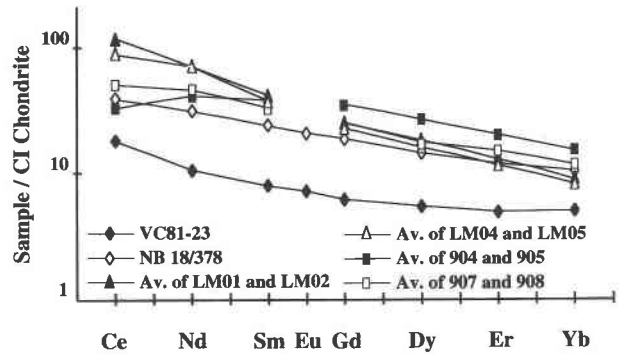


Fig. 14. Melt REE patterns calculated from orthopyroxene REE determined by isotope dilution and SIMS data. LM01/02 (norites) and LM04/05 (bronzitites) are from Lambert and Simmons (1987), determined by isotope dilution. Data on 904/905 (norites) and 907/908 (bronzitites) are determined by SIMS. Sills VC81 and NB18, which may represent parental melts, are included for comparison (REE data from Lambert and Simmons, 1988).

Whole-rock trace element abundances in bronzitites indicate a trapped liquid component between 1 and 6% (McCallum, 1984). Consequently, the postcumulus shift is small in most cases.

The following summarizes observations on the bronzitite-norite zone contact: (1) Norites immediately above the contact commonly contain pegmatitic and anorthositic segregations, and layering is folded and disturbed (Thurber and McCallum, 1990). (2) Selvages of chromite up to 3 mm thick are developed along the bronzitite-norite zone contact (Thurber and McCallum, 1990). (3) There is an increase in the amount of intercumulus plagioclase and augite in the uppermost 10 m of the bronzitite zone (Raedeke and McCallum, 1984). (4) Orthopyroxene is compositionally homogeneous throughout the bronzitite zone (Raedeke and McCallum, 1984). (5) There is a decrease in $Mg/(Mg + Fe)$ (up to 4 mol%), Cr_2O_3 , and Al_2O_3 and an increase in TiO_2 from bronzitite to norite (Raedeke, 1982; Lambert and Simmons, 1987; this study). (6) Intercumulus plagioclase in bronzitite has significantly higher $(Ce/Sm)_n$, $(Nd/Sm)_n$, and Eu/Eu^* relative to cumulus plagioclase in norite (Lambert and Simmons, 1988). (7) Orthopyroxenes in bronzitites and norites have similar absolute REE abundances, but orthopyroxene in bronzitites has slightly higher $(Ce/Yb)_n$ and smaller Eu anomalies. In the Mountain View area, bronzites in the single norite sample have distinctly higher Zr and Y abundances (this study).

Although no single observation is definitive, the weight of evidence favors the introduction of a batch of plagioclase-saturated melt (\pm intratelluric plagioclase) at the top of the bronzitite zone. Evidence for thermal erosion coupled with discontinuities in trace element abundances in minerals (particularly plagioclase) is particularly striking. Several of the observations, summarized above, are consistent with a model in which a loosely consolidated mush

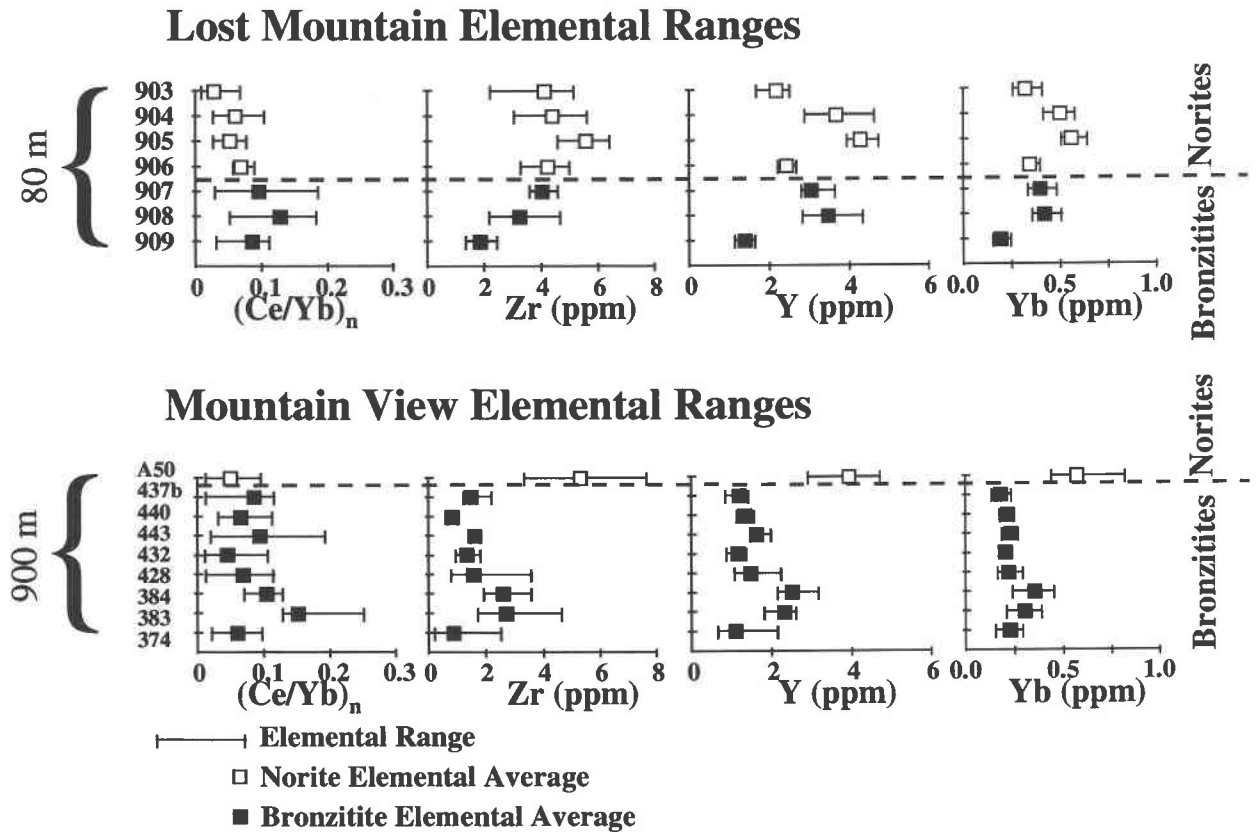


Fig. 15. Selected trace element data for the Lost Mountain and Mountain View sample suites plotted with respect to stratigraphic position. Data are presented in Tables 4 and 6. The Lost Mountain suite spans 80 m, whereas the Mountain View suite spans 900 m.

or suspension of orthopyroxene mixed with a batch of plagioclase-saturated magma. The chromite selvages appear to be the product of a reaction between orthopyroxene and a melt that was undersaturated in orthopyroxene. It is known from experimental studies that Cr originally contained within the orthopyroxene can be precipitated as chromite in the dissolution reaction (Brearley and Scarfe, 1986).

REE concentrations in liquids calculated on the basis of orthopyroxene REE data are similar to REE abundances in magnesian gabbro-noritic sills, lending support for Helz's (1985) conclusion that these sills would be suitable parental melts for the ultramafic series. On the other hand, mafic norite sills, which Helz also proposed as potential parental magmas, have REE abundances that lie below the range of calculated values.

ACKNOWLEDGMENTS

This research was supported by NASA grant NAGW-3347 and the Institute of Meteoritics (J.J.P., M.N.S., G.W.F.), and by NSF grant EAR-9406243 (I.S.M.). SIMS analyses were performed at the UNM/SNL Ion Microprobe Facility, a joint operation of the Institute of Meteoritics, University of New Mexico, and Sandia National Laboratories. We thank Graham Layne for technical help with the SIMS analyses. Constructive reviews were provided by David Lambert, David Lindstrom, and Patricia Loferski and are very much appreciated.

REFERENCES CITED

- Anders, E., and Grevesse, N. (1989) Abundances of the elements: Meteorite and solar. *Geochimica et Cosmochimica Acta*, 53, 197–214.
- Bonnichsen, B. (1969) Metamorphic pyroxenes and amphiboles in the Biwabik Iron Formation, Dunka River Area, Minnesota. *Mineralogical Society of America Special Paper*, 2, 217–239.
- Brearley, M., and Scarfe, C.M. (1986) Dissolution rates of upper mantle minerals in an alkali basalt melt at high pressure: An experimental study and implications for ultramafic xenolith survival. *Journal of Petrology*, 27, 1157–1182.
- Czamanske, G.K., and Zientek, M.L., Eds. (1985) *The Stillwater Complex, Montana: Geology and guide*, 396 p. Montana Bureau of Mines and Geology, Special Publication 92, Butte, Montana.
- DePaolo, D.J., and Wasserburg, G.J. (1979) Sm-Nd age of the Stillwater Complex and the mantle evolution curve for neodymium. *Geochimica et Cosmochimica Acta*, 43, 999–1008.
- Fowler, G.W., Papike, J.J., Spilde, M.N., and Shearer, C.K. (1994) Diogenites as asteroidal cumulates: Insights from orthopyroxene major and minor element chemistry. *Geochimica et Cosmochimica Acta*, 58, 3921–3929.
- Fowler, G.W., Shearer, C.K., and Papike, J.J. (1995) Diogenites as asteroidal cumulates: Insights from orthopyroxene trace element chemistry. *Geochimica et Cosmochimica Acta*, 59, 3071–3084.
- Helz, R.T. (1985) Compositions of fine-grained mafic rocks from sills and dikes associated with the Stillwater Complex. In G.K. Czamanske and M.L. Zientek, Eds., *The Stillwater Complex, Montana: Geology and guide*, p. 96–117. Montana Bureau of Mines and Geology, Special Publication 92, Butte, Montana.
- Hess, H.H. (1960) Stillwater igneous complex, Montana: A quantitative mineralogical study. *Geological Society of America Memoirs*, 80, 230 p.

- Irving, A.J., and Frey, F.A. (1984) Trace element abundances in megacrysts and their host basalts: Constraints on partition coefficients and megacryst genesis. *Geochimica et Cosmochimica Acta*, 48, 1201–1221.
- Kurat, G., Palme, H., Spettel, H., Hildegard, B., Hofmeister, H., Palme, C., and Wänke, H. (1980) Geochemistry of ultramafic xenoliths from Kapfenstein, Austria: Evidence for a variety of upper mantle processes. *Geochimica et Cosmochimica Acta*, 44, 45–60.
- Lambert, D.D. (1982) Geochemical evolution of the Stillwater Complex, Montana: Evidence for the formation of platinum-group element deposits in mafic layered intrusions, 274 p. Ph.D. thesis, Colorado School of Mines, Golden, Colorado.
- Lambert, D.D., and Simmons, E.C. (1987) Magma evolution in the Stillwater Complex, Montana: I. Rare-earth element evidence for the formation of the ultramafic series. *American Journal of Science*, 287, 1–32.
- (1988) Magma evolution in the Stillwater Complex, Montana: II. Rare earth element evidence for the formation of the J-M Reef. *Economic Geology*, 83, 1109–1126.
- Lambert, D.D., Walker, R.J., Morgan, J.W., Shirey, S.B., Carlson, R.W., Zientek, M.L., Lipin, B.R., Koski, M.S., and Cooper, R.L. (1994) Re-Os and Sm-Nd isotope geochemistry of the Stillwater Complex, Montana: Implications for the petrogenesis of the J-M Reef. *Journal of Petrology*, 35, 1717–1753.
- Loferski, P.J., and Arculus, R.J. (1993) Multiphase inclusions in plagioclase from anorthosites in the Stillwater Complex, Montana: Implications for the origin of anorthosites. *Contributions to Mineralogy and Petrology*, 114, 63–78.
- Mason, B., and Allen, R.O. (1973) Minor and trace elements in augite, hornblende and pyrope megacrysts from Kakanui, New Zealand. *New Zealand Journal of Geology and Geophysics*, 16, 935–947.
- McCallum, I.S. (1984) Estimation of trapped liquid contents in the Stillwater Complex. *Lunar and Planetary Science*, XV, 523–524.
- McCallum, I.S., Raedeke, L.D., and Mathez, E.A. (1980) Investigations of the Stillwater Complex: I. Stratigraphy and structure of the banded zone. *American Journal of Science*, 280-A, 59–87.
- McKay, G.A. (1989) Partitioning of rare earth elements between major silicate minerals and basaltic melts. In *Mineralogical Society of America Reviews in Mineralogy*, 21, 45–74.
- Papike, J.J., Fowler, G.W., and Shearer, C.K. (1994) Orthopyroxene as a recorder of lunar crust evolution: An ion microprobe investigation of Mg-suite norites. *American Mineralogist*, 79, 796–800.
- Pun, A., and Papike, J.J. (1995) Ion microprobe investigation of exsolved pyroxenes: Determination of minor and trace-element partition coefficients. *Geochimica et Cosmochimica Acta*, 59, 2279–2289.
- Raedeke, L.D. (1982) Petrogenesis of the Stillwater Complex, 212 p. Ph.D. thesis, University of Washington, Seattle, Washington.
- Raedeke, L.D., and McCallum, I.S. (1980) A comparison of fractionation trends in the lunar crust and the Stillwater Complex. In J.J. Papike and R.B. Merrill, Eds., *Proceedings of the Conference on the Lunar Highlands Crust*, p. 133–153.
- (1984) Investigations in the Stillwater Complex: II. Petrology and petrogenesis of the ultramafic series. *Journal of Petrology*, 25, 395–420.
- Shimizu, N., Semet, M.P., and Allégre, C.J. (1978) Geochemical applications of quantitative ion-microprobe analysis. *Geochimica et Cosmochimica Acta*, 42, 1321–1334.
- Spilde, M.N., Brearley, A.J., and Papike, J.J. (1993a) Alteration of plagioclase and pyroxene phenocrysts in a fissure fumarole, Valley of Ten Thousand Smokes, Alaska. *American Mineralogist*, 78, 1066–1081.
- Spilde, M.N., Papike, J.J., Layne, G.D., and McCallum, I.S. (1993b) Microbeam studies of core to rim variations in orthopyroxene from the Stillwater Complex, Montana. *Geological Society of America Abstracts with Programs*, 25, A-216.
- Stosch, H.-G. (1982) Rare earth element partitioning between minerals from anhydrous spinel peridotite xenoliths. *Geochimica et Cosmochimica Acta*, 46, 793–811.
- Thurber, M.W., and McCallum, I.S. (1990) The ultramafic series: Banded series contact in the Stillwater Complex: Evidence for thermal erosion. *Lunar and Planetary Science*, XXI, 1254–1255.

MANUSCRIPT RECEIVED FEBRUARY 20, 1995

MANUSCRIPT ACCEPTED JULY 17, 1995